Journal of The Electrochemical Society, **146** (7) 2533-2539 (1999)
S0013-4651(98)09-086-7 CCC: $7.00 © The Electrochemical Society, Inc.

Barrier Characteristics of Chemical Vapor Deposited Amorphous-like Tungsten Silicide with In Situ Nitrogen Plasma Treatment

Kow-Ming Chang, I-Chung Deng, Ta-Hsun Yeh, and Chien-Wen Shih

Department of Electronics Engineering and Institute of Electronics, National Chiao Tung University and National Nano Device Laboratory, Hsinchu, Taiwan

Our team investigated the characteristics of inserting an 80 nm amorphous-like $WSi_{1.6}N_{0.5}/WSi_{1.6}$ barrier layer between aluminum film and a shallow diode to retard aluminum and silicon interdiffusion. In one chamber without breaking vacuum, we used a nitrogen plasma treatment to stuff nitrogen atoms into the grain boundaries of amorphous-like tungsten silicide film. The nitrogen atoms eliminated the fast diffusion paths of film, thus giving the amorphous-like tungsten silicide film a smaller diffusion coefficient. We then examined the failure of diodes with amorphous-like $WSi_{1.6}N_{0.5}/WSi_{1.6}$ barriers which were annealed at 575°C for 30 min and which had leakage currents of 10^7 and 10^8 nA/cm^2. These diodes failed due to the diffusion of aluminum along the sidewalls of the barriers and the field oxide interface. In the search for a solution to this problem we investigated the use of tetraethylorthosilicate, which is known for its thermal stability as a stress buffer. In this experiment we used tetraethylorthosilicate to form a "contact array structure" which in turn prevented diode failure at 575°C annealing for 30 min, and furthermore, the diodes in the contact array structure only began to show evidence of degradation at 600°C.
© 1999 The Electrochemical Society. S0013-4651(98)09-086-7. All rights reserved.

Manuscript submitted September 25, 1998; revised manuscript received March 1, 1999.

A major problem encountered with Al metallizations occurs when Al and Si are in direct contact. The Al thin film is a polycrystalline structure that has grain boundaries, and these grain boundaries provide very fast diffusion paths for Si. After a significant quantity of Si atoms has diffused into the Al, the Al rapidly diffuses into the Si, thus filling the voids and forming pits and spikes in the Si substrate. These spikes/pits either increase the reverse current of junctions or short the shallow junction devices. One solution to reduce the spikes has been to replace pure Al with an Al-Si alloy. However, this solution is only workable on very deep junctions.[1] A second problem of the Al/Si alloy is precipitation of Si at the Al/Si interface during the cooling process of the sintering thermal cycle (nodule formation).[1,2] This phenomenon leads to an increase in the contact resistance or even to the complete blocking of the contact area in the submicron device.

Diffusion barriers, which prevent or retard diffusion, are classified into three types:[3-5] (*i*) passive barriers, (*ii*) sacrificial barriers, and (*iii*) stuffed barriers. Some barriers have two or three kinds of effects simultaneously.[4,6,7] Barriers made from refractory metals which have been treated with nitrogen or oxygen plasma can be more effective. This can be accomplished either by stuffing the barrier metal's grain boundaries with nitrogen or oxygen atoms or by the process of passivation, which creates a strong chemical bond.

Polycrystalline structures have grain boundaries that provide fast diffusion paths. However, diffusion through an amorphous material is often slower than through its polycrystalline analog. In this paper we compared the effectiveness of amorphous-like tungsten silicide (a-WSi_x) and columnar tungsten (c-W) in blocking Al and Si interaction. Further, because a nitride component adds more chemical stability than the refractory metal alone,[8-10] we also compared the effectiveness of this process with a-WSi_x and c-W in blocking Al and Si interaction. The nitridation process uses primarily either N_2 or NH_3 ambient.

Titanium nitride has also been studied extensively as a barrier material. It shows better adhesion than chemical vapor deposited (CVD) W to Si and SiO_2. It is also used as a glue layer to improve the adhesion of CVD W and/or WN_x films with Si. [11,12] However, sputtering behavior of WN_x can suffer the same reproducibility problems as TiN. These include impurities content, resistivity variation, and negative dc bias which may change the properties of film. (The reproducibility problem of TiN can be efficiently controlled by a commercial machine.) Kolawa et al.[13] compared the sputter deposition of TiN and WN_x. In their report they described various conditions such as radio frequency (rf) power, deposition rate, dc substrate bias, film composition, and oxygen concentration. Furthermore, other studies have shown that tungsten reveals more thermal stability than Ti. In addition, the WN_x film has the same stoichiometry when using different sputtering parameters. A WN_x layer is also a good etch-stop for the chlorine-based dry etching processes, unlike TiN. Both 80 nm thickness layers of TiN and $W_{67}N_{33}$ were sputtered by fixing the deposition rate as well as the gas composition and pressure. The unwanted compressive stress of TiN is two times stronger than that of $W_{67}N_{33}$ films.[14,15] Using CVD, WN_x, and TiN can easily make tensile stress by suitable deposition conditions.[16] Reid et al.[17] reported that W-Si-N barriers with approximately 50% nitrogen are able to prevent Al from spiking into the shallow-junction diodes at temperatures in excess of the melting point of Al. According to these properties then, we feel that the CVD tungsten silicide barrier is a more attractive candidate for ultralarge-scale-integrated (ULSI) diffusion barrier applications.

Experimental

The diodes used in this experiment were made on 6 in. (100) wafers which were cleaned by the standard RCA process. Field oxide of 500 nm was then grown on the substrate. The active regions were implanted with 3×10^{15} As^+ or BF_2^+ ions/cm^2 at an energy of 50 keV for n^+p or p^+n diodes, respectively. After annealing at 900°C for 30 min, the junction depths of the diodes were found to be about 0.3 and 0.35 μm for As^+ or BF_2^+, respectively. Furthermore, the annealing process at 900°C, either in a furnace or in a rapid thermal annealer, was used to remove defects and to activate the implanted doses.

Next, prior to the a-$WSi_{1.6}$ deposition or (for the contrasting side of the experiment) the c-W deposition, an in situ pretreatment was performed to remove the native oxide on the Si substrate at a pressure of 25 mTorr using NF_3/N_2 with a flow ratio of 24/72 sccm and 100 W rf power for 300 s. Then, blanket a-$WSi_{1.6}$ films of about 80 nm were deposited by a chemical vapor deposition system (ULVAC ERA-1000 system). The base pressure of the chamber was 10^{-6} Torr. The operating recipe for the amorphous-like film is described as follows: substrate temperature 300°C, total pressure 100 mTorr, and flow rates of SiH_4/WF_6 were 12.5/5 sccm. The deposition rate was about 448 nm/min. The c-W films with columnar structure were also deposited in this chamber and the flow rates of SiH_4/WF_6 were 9/20 sccm.

These CVD-W films and the nitridation process were executed in the same chamber without breaking vacuum. The a-$WSi_{1.6}N_{0.5}$/a-$WSi_{1.6}$ barrier layers were formed by CVD a-$WSi_{1.6}$ film exposure to N_2 plasma, and the nitridation parameters were 25 mTorr pressure, 100 W rf power with a N_2 flow rate of 100 sccm for 5 min; substrate temperature was 300°C. Subsequently, we covered the tung-

Downloaded on 2014-04-28 to IP 140.113.38.11 address. Redistribution subject to ECS terms of use (see ecsdl.org/site/terms_use) unless CC License in place (see abstract).

S0013-4651(98)09-086-7 CCC: $7.00 © The Electrochemical Society, Inc.

sten nitride (after the process of W-nitridation) with 500 nm of evaporated aluminum with breaking vacuum. Figure 1a shows the cross-sectional diagram of this diode. Figure 1b shows a diode with what our group calls a "contact array diode" structure. This is done by inserting 300 nm of tetraethylorthosilicate (TEOS) between the W and the Si substrate in such a way as to allow for a square array of contact points, which is the foundation of the "contact array diode." We reserved half of each wafer for material analysis; these halves did not contain patterns and were measured by X-ray diffraction (XRD), Rutherford backscattering spectroscopy (RBS), secondary ion mass spectrometry (SIMS), and X-ray photoelectron spectroscopy (XPS).

The efficiency of the diffusion barriers was determined by the variation of sheet resistance and from the leakage current of junction diodes at the following annealing temperatures: 500, 550, 575, and 600 for 30 min in N_2 ambient. The sheet resistance of barriers was measured by the TENCOR m-gap™ 300 which is a nine-point contactless measurement. The leakage current of the diodes was measured by the Hewlett Packard semiconductor parameter analyzer (HP4145B).

The crystalline structure analysis of the barrier films were carried out by XRD. An RBS of He^+ ions was used to characterize the interface after the furnace annealing. Furthermore, the surface morphologies and the cross sections were studied by scanning electron microscopy (SEM). The atomic concentrations of nitrogen in the a-$WSi_{1.6}N_{0.5}$ film were investigated by SIMS and their chemical bonding was investigated by XPS.

Results and Discussion

In our previous work,[18] we reported that a-WSi_x did not change its structure after in situ nitridation, even though nitrogen atoms in the a-WSi_x had the characteristics of stuffing in a diffusion barrier. In our present experiment, the annealed samples of the a-WSi_x/<Si> structure were investigated by RBS spectroscopy, which used an α-particle of 2 MeV and a detection angle of 160°. Figure 2a demonstrates the profiles of a-WSi_x on an Si substrate after annealing at 600 and 700°C for 30 min. Both profiles are almost the same as that of the as-deposited sample (not shown here). A diffraction pattern (curve a, Fig. 3) resembling the amorphous phase was identified, but no peaks resembling WSi_x were found. Furthermore, the concentration of silicon in the a-WSi_x film was quantified by an RBS analysis. The atomic ratio of silicon to tungsten is approximately 1.6 ($WSi_{1.6}$).

The resistivity of c-W films is 10 μΩ cm, which is much smaller than the a-$WSi_{1.6}$ films of 167 μΩ cm in this experiment. WSi_2 peaks formed after a-$WSi_{1.6}$ was annealed at 700°C for 30 min, as shown in Fig. 6. Upon comparing the annealed sample and an as-deposited sample with an RBS profile, we found that they retained the same RBS spectrum. The broader W peak of the sample (the dotted line in Fig. 2a) annealed at 700°C may be due to a thicker a-$WSi_{1.6}$ film than the other one annealed at 600°C. On the other hand, no platform was observed for c-W film after annealing at 600°C for 30 min. This implies that an almost pure W (i.e., no Si incorporation) was deposited by the c-W deposition recipe. We exposed the a-$WSi_{1.6}N_y$ film in

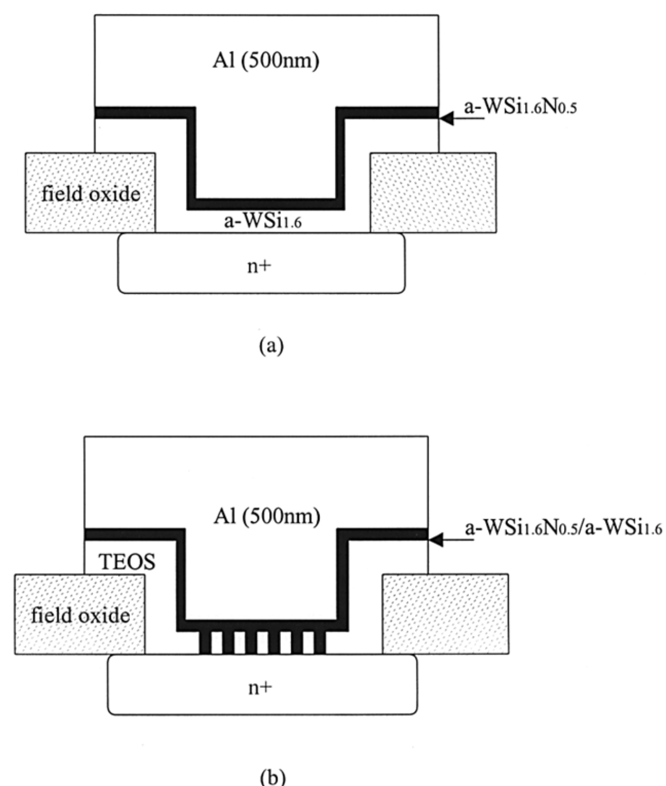

Figure 1. The cross section of diodes: (a) Al/a-$WSi_{1.6}N_{0.5}$/a-$WSi_{1.6}$/<Si> and (b) contact array diode.

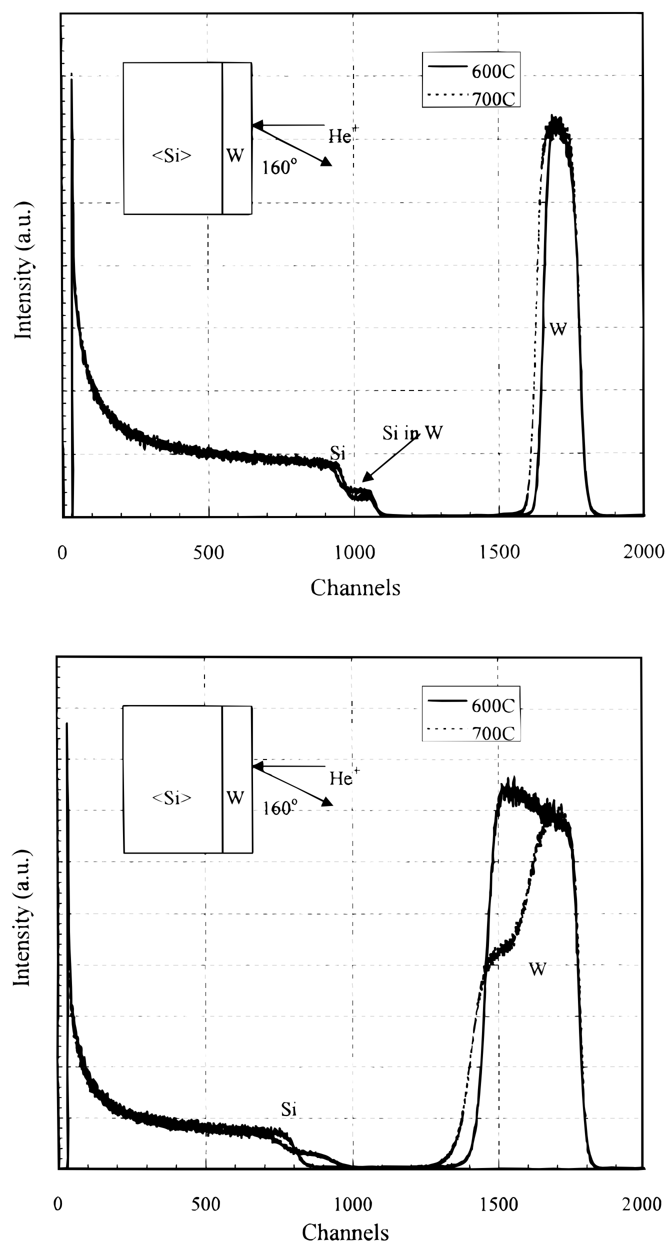

Figure 2. RBS spectra of (a, top) amorphous-like CVD-$WSi_{1.6}$ (a-$W_{1.6}$) layer on Si substrate and (b, bottom) columnar CVD-W (c-W) layer on Si substrate after annealing at various temperatures for 30 min.

Downloaded on 2014-04-28 to IP 140.113.38.11 address. Redistribution subject to ECS terms of use (see ecsdl.org/site/terms_use) unless CC License in place (see abstract).

S0013-4651(98)09-086-7 CCC: $7.00 © The Electrochemical Society, Inc.

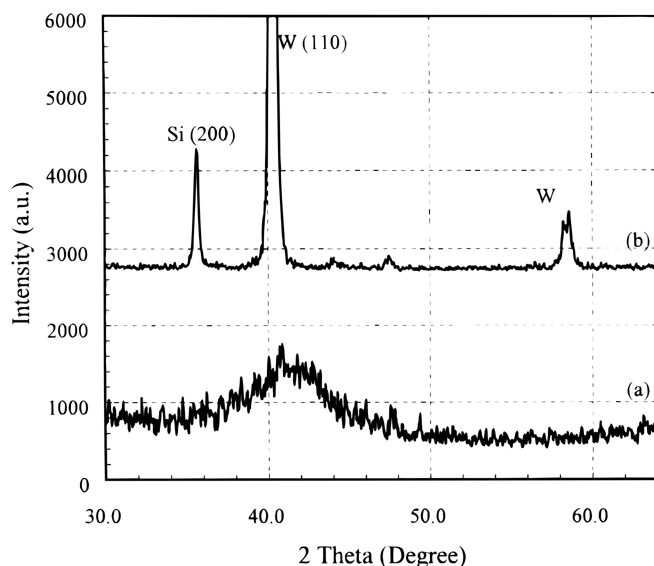

Figure 3. The XRD patterns of (a) amorphous-like CVD-$WSi_{1.6}$ (a-$W_{1.6}$) film and (b) columnar CVD-W (c-W) film.

N_2 plasma at 300°C for 5 min. The SIMS profile revealed that the upper 50 nm of the a-$WSi_{1.6}$ film was transformed to a-$WSi_{1.6}N_x$, as shown in Fig. 4. The N_{1S} spectrum reveals only one peak at 399.7 eV, as shown in Fig. 5, this is ascribed to the stuffing of nitrogen atoms or molecules in the grain boundaries of the a-$WSi_{1.6}$. Figure 5 indicates that the nitrogen and the tungsten do not have a strong covalent or ionic bond, so the nitrogen atoms or molecules are loosely attached to W atoms and act as a "stuffing" agent to block the diffusion paths. Therefore, the fast diffusion paths of the W grain boundaries were filled with nitrogen atoms, creating an a-WSi_xN_y layer with excellent barrier characteristics. However, the resistivity was increased to 198 μΩ cm. However, from XRD analysis, this film shows an amorphous peak. This contradicted with the XPS analysis of the stuffing of nitrogen atoms in grain boundaries of the a-$WSi_{1.6}$. Therefore, we propose that our tungsten film ($WSi_{1.6}$) contains WSi_x and amorphous-like tungsen simultaneously. We find that these disordered fine grains of tungsten in our tungsten film do not cause any detectable tungsten peaks. We suggested that nitrogen atoms stuff these grain boundaries of fine grain tungsten. This is the reason why there is only one N_{1S} peak at 399.7 eV. Also, the $W_{4f7/2}$ and $W_{4f5/2}$ peaks are situated at the same position after the process of nitridation. This implies that the chemical bonds of a-$WSi_{1.6}$ film do not change too much due to nitridation. We have named it "amorphous-like" rather than "amorphous." After the nitridation process, the percentage of nitrogen atoms is half of W atoms by XPS analysis ($WSi_{1.6}N_{0.5}$) and the percentage of oxygen in our film is about 21%. The higher contamination of oxygen may be due to surface oxide.

Now we look at the data for the c-W samples. After annealing the c-W sample at 700°C for 30 min (Fig. 2b), we find that the high-energy edge of the Si peak and the low-energy edge of the c-W peak shifted toward the higher and the lower backscattered energies, respectively. Note that RBS peak-height analysis also shows that WSi_2 is forming. The profiles of Si and W peaks (solid line of Fig. 2b) show that the Si atoms diffuse into the c-W film and the c-W film converts to tungsten disilicide (as shown in Fig. 6b). This implies that the grains in the c-W film appear to be wrapped with Si and to be transforming progressively into WSi_x. XRD patterns were used to analyze the growth of the WSi_x crystal structures with different samples at various annealing conditions.

Furthermore, Fig. 7a and b, respectively, show the RBS characteristics of the Al/c-W/<Si> samples after annealing at 600°C for 30 min. We clearly see that Al/barriers/<Si> with an a-$WSi_{1.6}$ film has a better thermal stability than c-W film. Compared with the W peak of the Al/c-W/<Si> sample (in Fig. 7b), the W peak of the Al/a-$WSi_{1.6}$/<Si> sample (in Fig. 7a) was much further away from the high-energy edge. On the other hand, the case of the Al/c-W/<Si> sample in Fig. 7b shows that all the peaks become significantly broader and closer after annealing at 600°C for 30 min. This is a result of the Al and Si atoms interdiffusing along their grain boundaries. When an a-$WSi_{1.6}N_{0.5}$ barrier layer is formed on the tungsten surface, it can avoid the harmful diffusions of Al and W at the Al/a-$WSi_{1.6}N_{0.5}$ interface. This nitride thin film improves the thermal stability of the contact system, because the nitrogen atoms occupy the grain boundaries[19] and the barrier layer.

Previously it was reported by So et al.[8] that when annealing Al/$W_{80}N_{20}$/<Si> at 600°C for 30 min the Si and Al atoms diffused into each other. It was noted here that Al film was in situ deposited on $W_{80}N_{20}$ with no vacuum break. In the next part of their experiments, they substituted Si substrate with SiO_2 substrate. With this

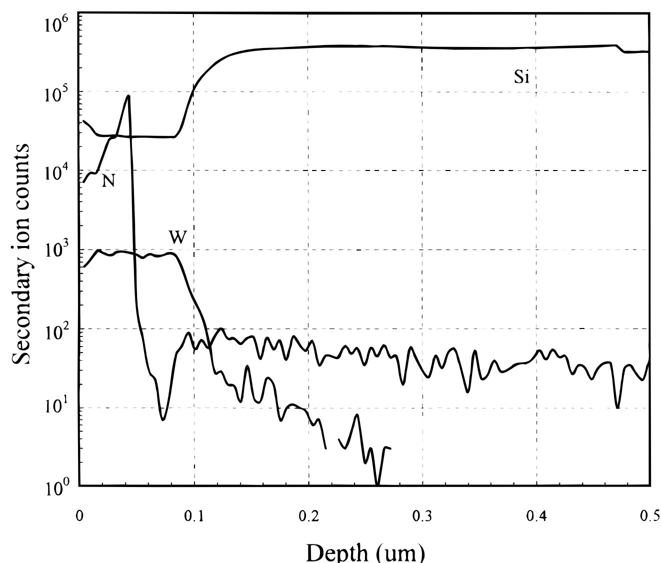

Figure 4. SIMS depth profiles of a-$WSi_{1.6}N_{0.5}$/a-$WSi_{1.6}$/<Si> multilayer formed by nitrogen plasma exposure at 300°C for 5 min on 120 nm thick CVD a-$WSi_{1.6}$ film.

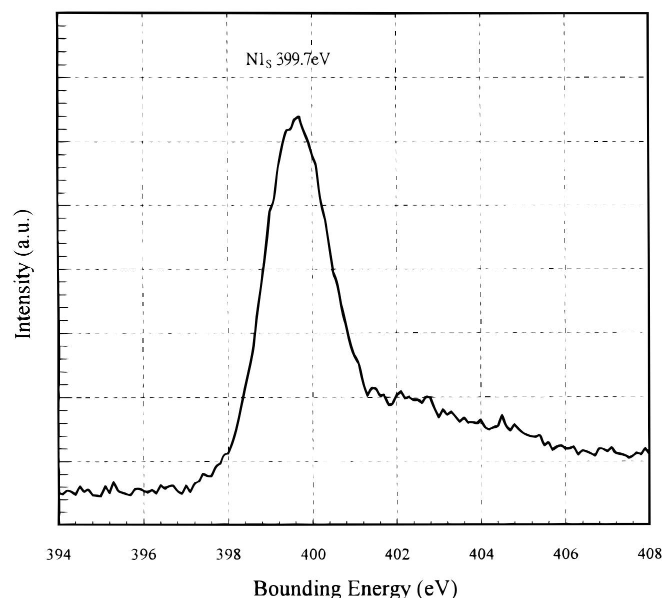

Figure 5. N_{1S} XPS spectrum of amorphous-like a-$WSi_{1.6}N_{0.5}$ layer.

Downloaded on 2014-04-28 to IP 140.113.38.11 address. Redistribution subject to ECS terms of use (see ecsdl.org/site/terms_use) unless CC License in place (see abstract).

S0013-4651(98)09-086-7 CCC: $7.00 © The Electrochemical Society, Inc.

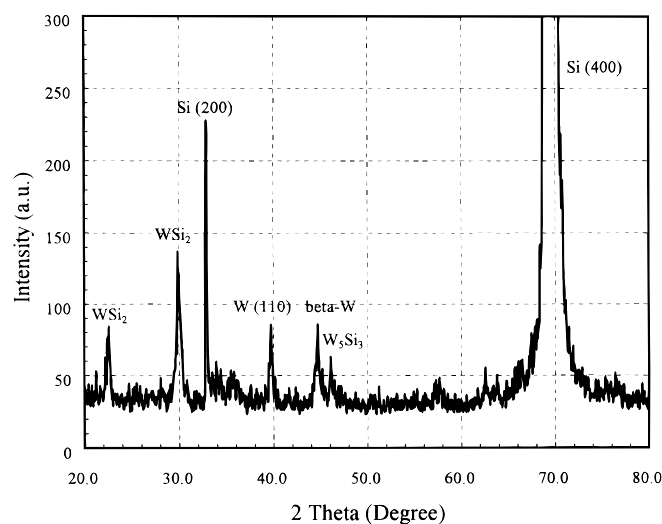

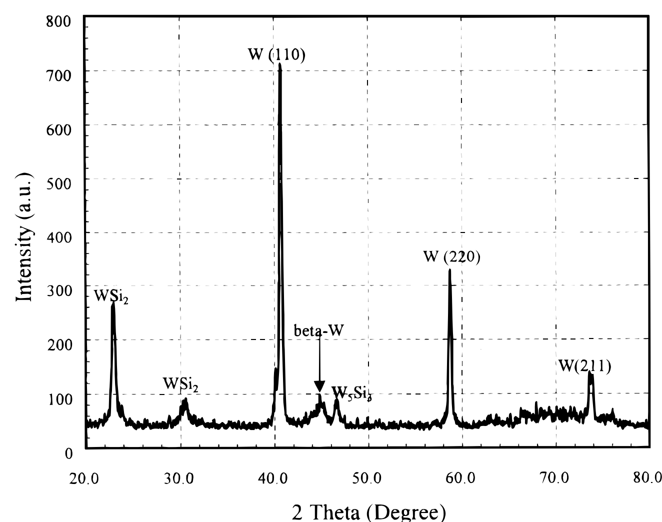

Figure 6. XRD patterns of (a, top) a-$WSi_{1.6}$ film on Si substrate and (b, bottom) c-W film on Si substrate after annealing at 700°C.

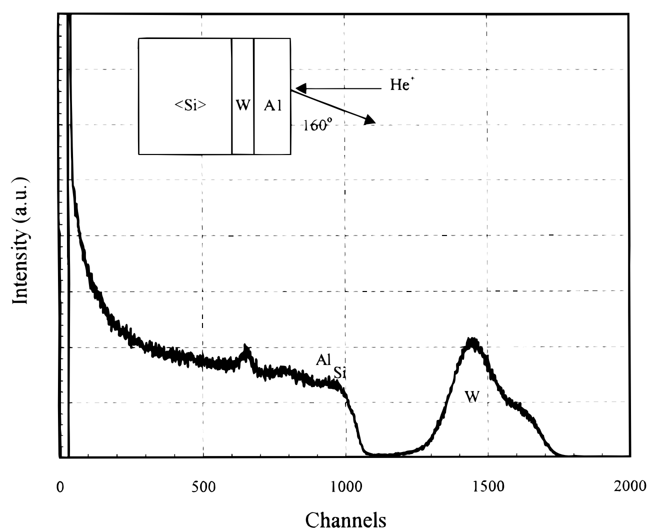

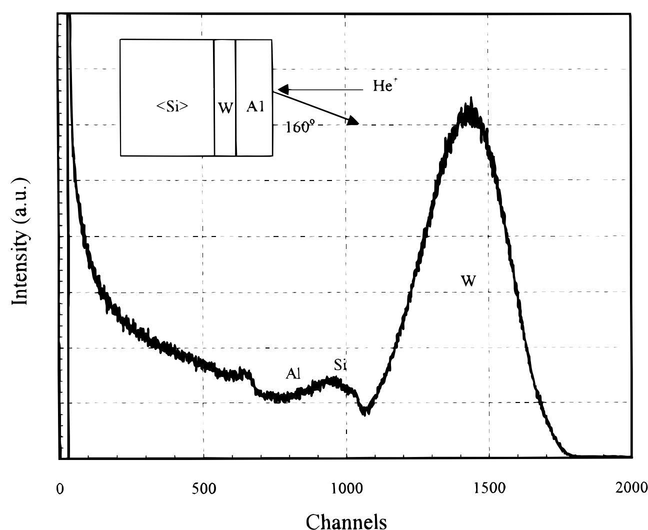

Figure 7. RBS pictures of (a, top) Al/a-$WSi_{1.6}$/<Si> and (b, bottom) Al/c-W/<Si> after annealing at 600°C for 30 min.

SiO_2 substrate they found that they could not detect any metallurgical interactions between the Al and the $W_{80}N_{20}$. They then compare the results of the Al/$W_{80}N_{20}$/<SiO_2> sample with the Al/$W_{80}N_{20}$/<Si> sample and only say that the failure of the Al/$W_{80}N_{20}$/<Si> sample was not due to the consumption of the $W_{80}N_{20}$ layer by Al to form WAl_{12}.[8] In our work, however, we found that when we annealed an a-$WSi_{1.6}N_{0.5}$/a-$WSi_{1.6}$/<Si> sample at 600°C for 30 min, it remained stable. In further a-$WSi_{1.6}N_{0.5}$/a-$WSi_{1.6}$/<Si> samples we observed that the small WSi_2 peaks began to appear at 700°C. We deduce that these small peaks of WSi_2 are the result of recrystallization of a-WSi_x. In Table I we give the qualitative analysis of the XRD and RBS results after various annealing

Table I. Thermal stability of layered structures.

Annealing conditions	Al/C-W/<Si>		Al/a-$WSi_{1.6}$/<Si>		Al/a-$WSi_{1.6}N_{0.5}$/ a-$WSi_{1.,6}$/<Si>		c-W/<Si>		a-$WSi_{1.6}$/<Si>	
T (°C)//*t* (min)	XRD	RBS	XRD	RBS	XRD	RBS	XRD	RBS	XRD	RBS
550/30	WSi_2, W(Si, Al)$_2$[a]	✕	WSi_2, W(Si, Al)$_2$	✕	✓	✕	✓	✕	✓	✕
550/90	WSi_2, W(Si, Al)$_2$	W, Al, Si	WSi_2, W(Si, Al)$_2$	W at surface	✓	✓	✓	✕	✓	✕
600/30	WSi_2, W(Si, Al)$_2$	✕	WSi_2, W(Si, Al)$_2$	✕	WSi_2, W(Si, Al)$_2$	✕	✓	✕	✓	✕
600/90	WSi_2, W(Si, Al)$_2$	W, Al, Si	WSi_2, W(Si, Al)$_2$	W, Al, Si	WSi_2, W(Si, Al)$_2$	W, Al, Si	✓	✕	✓	✕
700//30	✕	✕	✕	✕	✕	✕	WSi_2	W, Si	WSi_2	✓

[a] W(Si, Al)$_2$ peak consists of Al(2, 00), WSi_2(103), and WAl_{12}(321).
✕ Data absent.
✓ No interdiffusion or WSi_2/S(Si,Al)$_2$ peaks are found.

Downloaded on 2014-04-28 to IP 140.113.38.11 address. Redistribution subject to ECS terms of use (see ecsdl.org/site/terms_use) unless CC License in place (see abstract).

S0013-4651(98)09-086-7 CCC: $7.00 © The Electrochemical Society, Inc.

conditions. This proves that without the Al deposition, the bilayer barrier of a-$WSi_{1.6}N_{0.5}$/a-$WSi_{1.6}$ has a stable interface below 700°C. Therefore, we suggest that the cause of the failure mechanism of So's sample was the result of Al reducing the thermal stability of the W-Si interface.

Figure 8 reveals the sheet resistance variations in three types of tungsten films deposited on Si substrate. First we see that the sheet resistance of the c-W increased steadily at temperatures over 650°C. This increasing sheet resistance is due to Si atoms diffusing into the c-W film. Then we see that the sheet resistance of the a-$WSi_{1.6}$ increased dramatically at 550°C and decreased at 700°C. The high-sheet-resistance region of the a-$WSi_{1.6}$ may be due to the phase transformation of the WSi_x.[20,21] Last, we see that the structure of c-W/a-$WSi_{1.6}N_{0.5}$/a-$WSi_{1.6}$/<Si> has an excellent thermal stability which changed very little even when annealed at 750°C for 30 min. This shows that the diffusion of Si atoms through the a-$WSi_{1.6}N_{0.5}$/a-$WSi_{1.6}$ bilayer is almost undetectable by sheet resistance measurement even when annealed at 750°C for 30 min. No change was observed in the nitrogen signal up to annealing temperature of 700°C by SIMS depth profile. Some authors[14] also show that nitrogen signal is still stable after annealing temperature up to 800°C in a vacuum chamber.

Next we examined the Al penetration in a test vehicle of a shallow n^+p or p^+n junction diode using an HP4145B. Shallow junction diodes are probably the most sensitive devices for testing the performance of diffusion barriers. A tiny metal spike or nonuniform reaction can cause a high reverse leakage current or a junction short circuit. Figure 9 shows the junction leakage current of the Al/a-$WSi_{1.6}N_{0.5}$/a-$WSi_{1.6}$/<Si> after annealing for 30 min. (The total thickness of the a-$WSi_{1.6}N_{0.5}$/a-$WSi_{1.6}$ barrier was 80 nm.) The leakage currents were measured at a reverse bias of 5 V on the diodes with a junction area of 2 × 2 mm. The samples of the shallow junction n^+p or p^+n diodes were formed by the rapid thermal anneal (RTA) process at 900 for 30 min. A random sampling of 50 diodes of the Al/a-$WSi_{1.6}N_{0.5}$/a-$WSi_{1.6}$/<Si> structure which was annealed at 550°C for 30 min showed a leakage of less than 10^3 nA/cm^2. In addition, at an annealing temperature of 575°C for 30 min, the same type of sample (as shown in Fig. 9) had a leakage current density of less than 10^3 nA/cm^2 in 62% of the random sampling of diodes. As can be seen, all the diodes failed after annealing at 600°C for 30 min.

When we observe these samples, which were annealed at 575°C, with SEM (Fig. 10), we see that square pits appear around the outlines of the failed diodes. This implies that the failure of the diodes at 10^7 and 10^8 nA/cm^2 in Fig. 9 was due to the diffusion of Al along the sidewalls of the barrier and the field oxide interface.[22] We ascribe the high stress on the corner of field oxide to be the cause of the fast diffusion paths along the sidewalls of the barrier and the field oxide interface. Al pass through these fast diffusion paths of the barrier across the contact step. Moreover, all diodes failed after annealing at 600°C for 30 min, in which we observed square pits not only around the outlines of the diodes but also in the active regions of the diodes. The square pits on the surface (Fig. 10) are due to the Al atoms diffusing into the Si substrate.

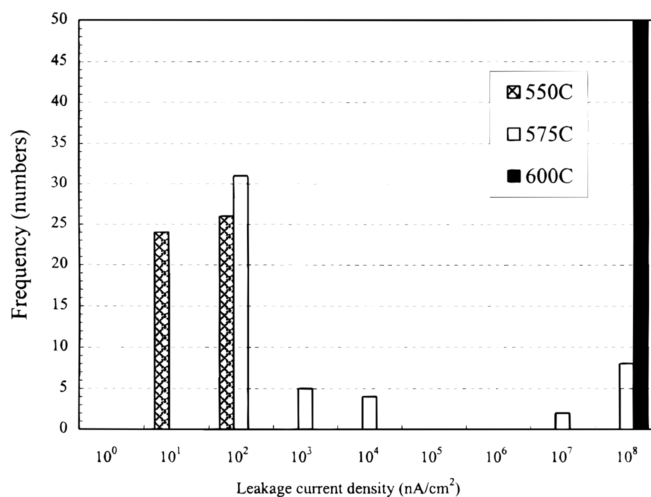

Figure 9. The statistical failures of accumulation diodes Al/a-$WSi_{1.6}N_{0.5}$/a-$WSi_{1.6}$/<Si> after annealing at various temperatures for 30 min.

In Table II we observed (with SEM) the surface morphologies of the three main structures in our experiment after annealing at 550°C and 600°C for 30 min. Microsized bubbles were found in the Al/a-$WSi_{1.6}$ and Al/a-$WSi_{1.6}N_{0.5}$/a-$WSi_{1.6}$ samples; none were found on the Al/<Si> diodes. This implies that the micron-sized bubbles are due to a partial loss of adhesion between the Al and the a-$WSi_{1.6}$ (or a-$WSi_{1.6}N_{0.5}$). Figure 11 shows photos of the thermal treatment after the removal of the Al. The structures we developed for this part of the experiment were Al/a-$WSi_{1.6}$/<Si> (Fig. 11a and b) and Al/a-$WSi_{1.6}N_{0.5}$/a-$WSi_{1.6}$/<Si> (Fig. 11c and d). In Fig. 11a, b, and d the square pits observed are junction spikes; they will short the diodes. When an a-$WSi_{1.6}$ film was inserted between the Al layer and the Si substrate (Fig. 11a), junction spikes were formed after annealing at 550°C for 30 min. Then after the Al film was removed, it was found that the surface showed many granular particles. These granular par-

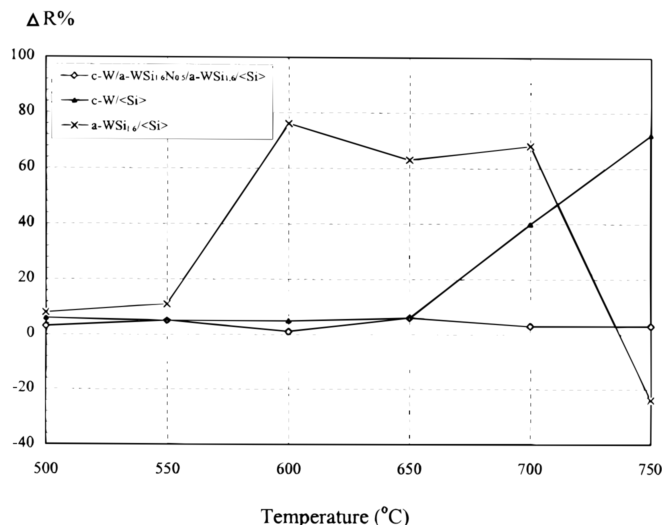

Figure 8. Change of sheet resistance of three structural samples after in N_2 ambient at various temperatures for 30 min.

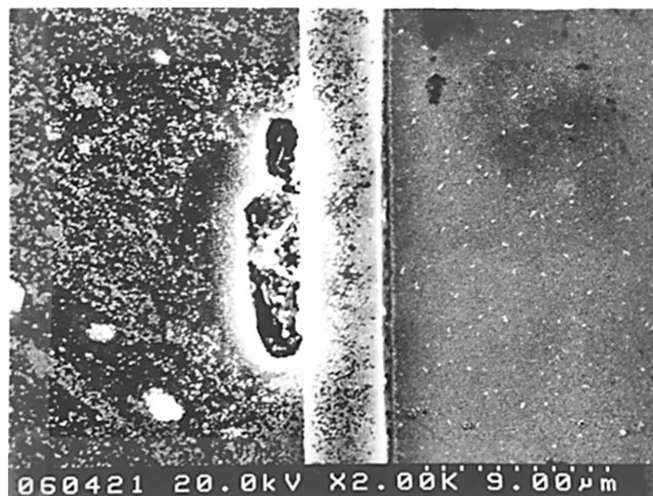

Figure 10. The square pits at the contact step of failures diode after annealing at 575°C for 30 min.

Downloaded on 2014-04-28 to IP 140.113.38.11 address. Redistribution subject to ECS terms of use (see ecsdl.org/site/terms_use) unless CC License in place (see abstract).

S0013-4651(98)09-086-7 CCC: $7.00 © The Electrochemical Society, Inc.

Table II. Inspection of the surface morphology.

	Al/<Si>		Al/a-$WSi_{1.6}$/ <Si>		Al/A-$WSi_{1.6}N_{0.5}$/ a-$WSi_{1.6}$/<Si>	
	550°C	600°C	550°C	600°C	550°C	600°C
Square pits	✓	✓	✓	✓	×	✓
Microbubble	×	×	✓	✓	✓	✓
Droplet	✓	✓	×	✓	×	✓
Granular Particles	×	×	✓	×	×	×

× Observed.
✓ Unobserved.

ticles may be caused by the residual tungsten film after the reaction with Al. This happens because the upper surface of the a-$WSi_{1.6}$ film which is in direct contact with the Al forms a WAl_{12} compound. This WAl_{12} compound was also stripped away during the Al wet etching process. In Fig. 11b, after annealing the sample at 600°C for 30 min we see (after Al wet etching process) that the a-$WSi_{1.6}$ film was almost totally consumed in a reaction with the Al; no granular particles could be seen as well. In Fig. 11c, however, the a-$WSi_{1.6}N_{0.5}$/a-$WSi_{1.6}$ barrier demonstrated excellent barrier behavior at a 550°C annealing for 30 min. As can be seen, it exhibits a smooth surface after the Al film was stripped in the wet etching process.

Furthermore, as seen in Fig. 12, when the a-$WSi_{1.6}N_{0.5}$/a-$WSi_{1.6}$ barrier is laid down with our "contact array diode" structure, the diodes were clearly more stable than the traditional structure of Fig. 1a. After annealing the contact array diode structure sample for 30 min at 575°C and then random-testing the diodes with a reverse bias of 5 V, an approximate 10^{-8} A/cm^2 leakage current was found. One step further, Fig. 12 shows that the degradation at a 600°C annealing temperature for 30 min was also considerably less than in the traditional structure of Fig. 1a. The reduction of the leakage current of the contact array diodes is partially due to TEOS, which can reduce the stress on the corner of the field oxide.

Conclusion

An amorphous-like (a-$WSi_{1.6}$) film, an interconnection material, was inserted between an Al and Si substrate as a barrier layer. Next,

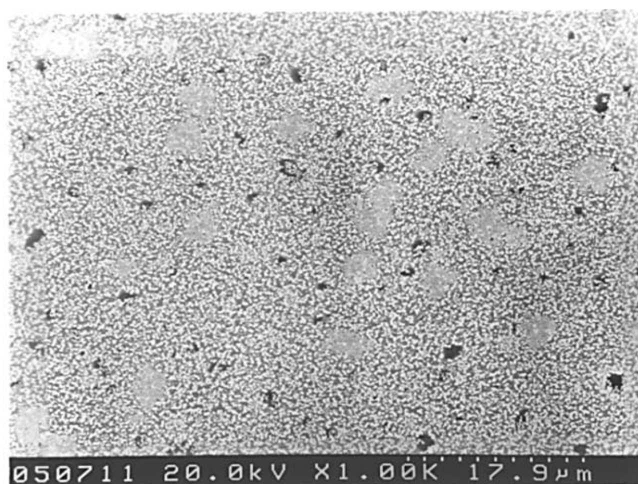

(a)

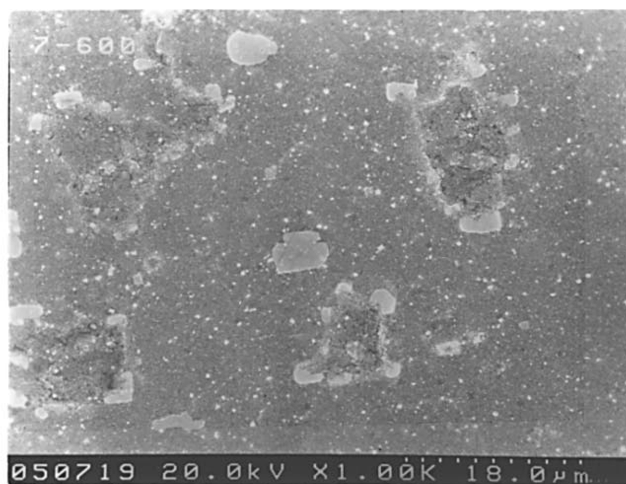

(b)

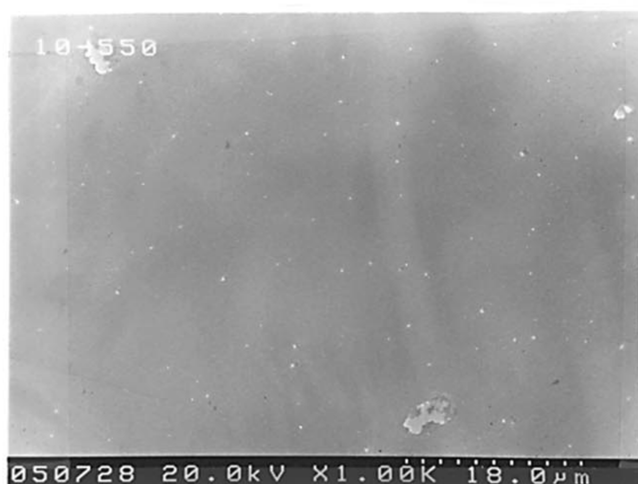

(c)

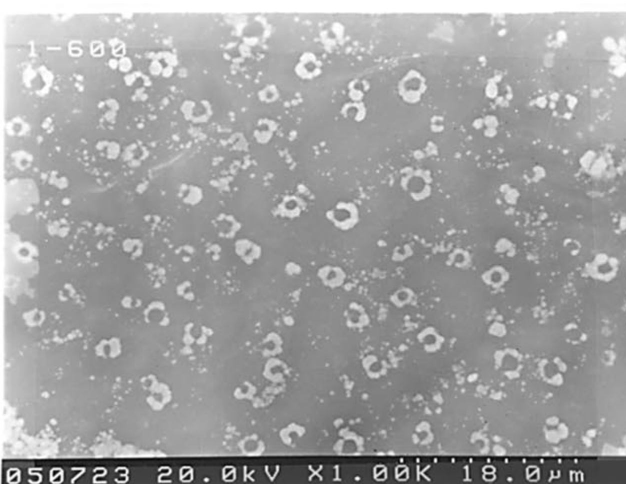

(d)

Figure 11. The different structure of (a) Al/a-$WSi_{1.6}$/<Si> annealed at 550°C, (b) Al/a-$WSi_{1.6}$/<Si> annealed at 600°C, (c) Al/a-$WSi_{1.6}N_{0.5}$/a-$WSi_{1.6}$/<Si> annealed at 550°C, and (d) Al/a-$WSi_{1.6}N_{0.5}$/a-$WSi_{1.6}$/<Si> annealed at 600°C for 30 min.

Downloaded on 2014-04-28 to IP 140.113.38.11 address. Redistribution subject to ECS terms of use (see ecsdl.org/site/terms_use) unless CC License in place (see abstract).

S0013-4651(98)09-086-7 CCC: $7.00 © The Electrochemical Society, Inc.

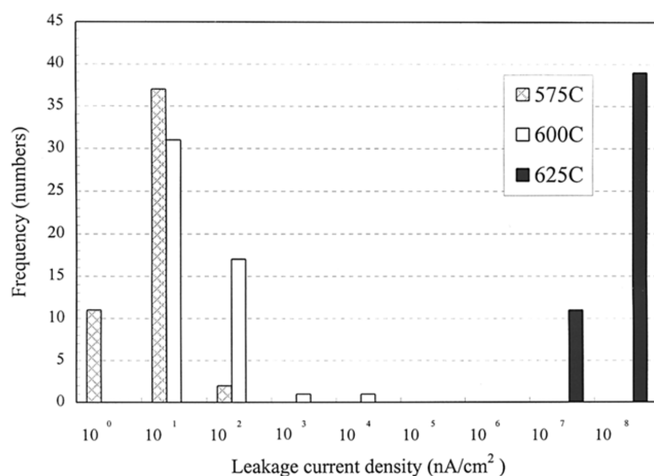

Figure 12. The statistical failures of accumulation diodes with contact array after annealing at various temperatures for 30 min.

the a-$WSi_{1.6}$/<Si> was subjected to a nitridation process. The upper 50 nm of the a-$WSi_{1.6}$ layer was then transformed to a-$WSi_{1.6}N_{0.5}$. We then found that this a-$WSi_{1.6}N_{0.5}$/a-$WSi_{1.6}$/<Si> structure remained stable even at an annealing temperature of 700°C for 30 min. However, when Al was deposited on this a-$WSi_{1.6}N_{0.5}$/a-$WSi_{1.6}$/<Si> structure we found that annealing above 600°C caused the failure mechanism of the Al/a-$WSi_{1.6}N_{0.5}$/a-$WSi_{1.6}$/<Si> structure. This is due to two problems: (*i*) the barrier destabilization is due to Al channels through local weak spots in the barrier. This caused a reduction of the thermal stability of the a-$WSi_{1.6}$/<Si> interface. This in turn caused the Si to diffuse toward the surface. Thus, the W-Al-Si compound was formed. (*ii*) At above a 577°C annealing temperature, Si and Al have high reactivity to each other. Therefore, Al atoms penetrate into the a-$WSi_{1.6}N_{0.5}$ and form a W-Al compound.

To suppress the (above-mentioned) Si-Al interaction, a-$WSi_{1.6}$ film is, in our view, far superior to the traditional c-W film. We have shown that an a-$WSi_{1.6}$/<Si> interface is stable up to an annealing temperature of 700°C for 30 min, as opposed to an annealing temperature of 600°C for c-W film. Also, the thermal stability of the Al/a-$WSi_{1.6}$ interface was improved. Next we see that after a nitrogen plasma treatment to the a-$WSi_{1.6}$ film the a-$WSi_{1.6}N_{0.5}$/a-$WSi_{1.6}$ barrier is much better at retarding the formation of WAl_{12}.

Next, the n^+p shallow junction contact array diodes in the Al/a-$WSi_{1.6}N_{0.5}$/a-$WSi_{1.6}$/<Si> structure demonstrated much lower junction leakage current (after annealing at 575°C for 30 min) than typical diodes. This is because the TEOS in the Al/a-$WSi_{1.6}N_{0.5}$/a-$WSi_{1.6}$/<Si> structure reduces the poor adhesion at the sidewall interface of the SiO_2 and a-$WSi_{1.6}N_{0.5}$/a-$WSi_{1.6}$ barrier and it also reduced the high stress on the corner of the field oxide. The development of high stress on the corner of the field oxide causes the fast diffusion paths along the sidewalls of the barrier and the field oxide interface. From this data we can say that a-$WSi_{1.6}N_{0.5}$/a-$WSi_{1.6}$ is an excellent diffusion barrier for ULSI application.

Acknowledgments

This work is supported by the National Science Council under grant NSC86-2215-E-009-047. This paper was revised by Mr. Michael S. Drummond.

National Chiao Tung University assisted in meeting the publication costs of this article.

Reference

1. P. A. Totta and R. P. Sopher, *IBM J. Res. Develop.,* **13,** 226 (1969).
2. R. Furlan, J. Van der Spiegel, and J. W. Swart, *J. Electrochem. Soc.,* **138,** 2377 (1991).
3. S. Wolf, *Silicon Process for the VLSI Era,* Vol. 2, pp.122-123, Lattice Press, CA (1990).
4. J. R. Shappirio, *Solid State Technol.,* **28,** 161 (1985).
5. M-A. Nicolet and M. Bartur, *J. Vac. Sci. Technol.,* **19,** 786 (1981).
6. S.-L. Zhang, U. Smith, R. Buchta, and M. Östling, *J. Appl. Phys.,* **69,** 213 (1991).
7. F. Meyer, D. Bouchier, A. Benhocine, and G. Gautherin, *Appl. Surf. Sci.,* **53,** 82 (1991).
8. F. C. T. So, E. Kolawa, X.-A. Zhao, E. T-S. Pan, and M.-A. Nicolet, *J. Appl. Phys.,* **64,** 2787 (1988).
9. E. Kolawa, F. C. T. So, J. L. Tandon, and M.-A. Nicolet, *J. Electrochem. Soc.,* **134,** 1759 (1987).
10. W. B. Nowak, R. Keukelaar, W. Wang, and A. R. Nyaiesh, *J. Vac. Sci. Technol.,* **A3,** 2242 (1985).
11. M. Wittmer, *J. Vac. Sci. Technol.,* **A3,** 1797 (1985).
12. A. Sherman, *J. Electrochem. Soc.,* **137,** 1892 (1990).
13. E. Kolawa, F. C. T. So, X.-A. Zhao, and M.-A. Nicolet, in *Tungsten and Other Refractory Metals for VLSI Applications II,* E. K. Broadent, Editor, p. 311, Materials Research Society, Pittsburgh, PA (1987).
14. H. P. Kattelus, E. Kolawa, K. Affolter, and M-A. Nicolet, *J. Vac. Sci. Technol.,* **A3,** 2246 (1985).
15. P. J. Pokela, C.-K. Kwok, S. Raud, and M.-A. Nicolet, *Appl. Surf. Sci.,* **53,** 364 (1991).
16. J. E. J. Schmitz, *Chemical Vapor Deposition of Tungsten and Tungsten Silicides for VLSI/ULSI Applications,* pp. 98-102, Noyes Publication, Park Ridge, NJ (1991).
17. J. S. Reid, E. Kolawa, C. M. Garland, M. -A. Nicolet, F. Cardone, D. Gupta, and R. P. Ruiz, *J. Appl. Phys.,* **79,** 1109 (1996).
18. K.-M. Chang, T.-H. Yeh, and I-C. Deng, *J. Appl. Phys.,* **81,** 3670 (1997).
19. A. Noya, M. Takeyama, K. Sasaki, E. Aoyagi, and K. Hiraga, *Jpn. J. Appl. Phys.,* **33,** 1528 (1994).
20. S. P. Murarka, M. H. Read, C. J. Doherty, and D. B. Fraser, *J. Electrochem. Soc.,* **129,** 293 (1982).
21. T. I. Kamins, S. S. Laderman, D. J. Coulman, and J. E. Turner, *J. Electrochem. Soc.,* **133,** 1438 (1986).
22. T. Fujii, T. Fujita, and T. Kouzaki, *J. Electrochem. Soc.,* **139,** 835 (1992).

Downloaded on 2014-04-28 to IP 140.113.38.11 address. Redistribution subject to ECS terms of use (see ecsdl.org/site/terms_use) unless CC License in place (see abstract).